Integral transform method solution for heat transfer in polymer melt flow in a parallel plate single screw channel with periodic inlet temperature

L.X. Bu, Y. Agbessi, J. Biglione, Yves Bereaux, Jean-Yves Charmeau

Version of Record: https://www.sciencedirect.com/science/article/pii/S1290072919301966
Manuscript_d2e44ccc05b2b624eaef741ffba07d7c

Integral transform method solution for heat transfer in polymer melt flow in a parallel plate single screw channel with periodic inlet temperature

L. X. Bu[b], Y. Agbessi[c], J. Biglione[b], Y. Béreaux[a,*], J.-Y. Charmeau[c]

[a] *Université de Nantes, GEPEA UMR 6229, IUT de Nantes, 2 av. Pr. Rouxel, France*
[b] *Université de Lyon, INSA-Lyon LaMCoS UMR 5259, 85 rue H. Becquerel, 01100 Oyonnax, France*
[c] *Université de Lyon, INSA-Lyon, IMP UMR 5223, Site de Plasturgie, 85 rue H. Becquerel, 01100 Oyonnax, France*

Abstract

This work investigates the capacity of a particular class of flows, namely drag and pressure driven flows, to propagate and distorts a transient sinusoidal temperature disturbance occurring at the inlet of the metering zone of a polymer processing screw channel. The integral transform method is applied to the forced convection heat transfer problem in a parallel plate channel with a general drag and pressure driven flow velocity profile for a Newtonian fluid, with the pressure gradient as an adjustable flow parameter. We follow closely the procedure outlined by Cotta and Özişik in their seminal paper [5]. We found that the knowledge of the lowest eigenvalue in the solution is sufficient to characterise the dampening efficiency of an inlet temperature fluctuation by the flow and that a higher level of positive pressure difference is indeed improving the thermal homogeneity in the flow. Moreover, we found that for any given flow, the higher frequency disturbances are dispersed more efficiently than the lower frequency disturbances.

Keywords: periodic inlet temperature, integral transform method, drag and pressure driven flow

1. Introduction

Single-screw plastication, used in extrusion and in injection moulding, is a major way of processing commodity thermoplastics. In these polymer shaping processes, a high level of reliability is usually achieved which makes this process ideally suited to mass market production. Nonetheless, process fluctuations still appear that make part quality control an everyday issue. Among the possible processes fluctuations, thermal fluctuations occurring at the plastication stage, which is early on in the polymer shaping process, could well be the cause for a temperature perturbation that will be carried to the part all the way through the die in extrusion or through the mould in injection moulding.

During the plastication phase, the polymeric material is melted by the combined effects of shear-induced self heating (viscous dissipation) and heat conduction coming from the barrel. Once the polymer is completely melted, a combined drag and pressure difference flow is imparted onto the molten polymer along the last zone of the screw channel, the so-called metering zone. The very high viscosity of molten polymers insure that the flow must be laminar and that the Reynolds number is negligible. The low thermal diffusion coefficient of

Preprint submitted to International Journal of Thermal Sciences *September 9, 2019*
*Corresponding author
Email address: yves.bereaux@univ-nantes.fr (Y. Béreaux)

molten polymers implies that convection is dominant over diffusion and leads to large Peclet numbers. However, the screw channel length is large enough for the flow to present significant diffusion effects. Indeed, calculations for frequently encountered single screw show that the residence time is one tenth of the thermal diffusion time, owing to the very low thermal diffusion of polymers.

Therefore, the main objective of this work is to study the capacity of this particular class of flows to dampen any transient inlet temperature disturbances occurring at the beginning of the metering zone of the screw channel. In particular, in this class of flows, the level of backpressure is a process parameter that can be set to a chosen value, in order to change the flow configuration. It is well known in polymer processing that a higher level of backpressure, *i.e.* a positive pressure difference, will increase the level of shear rate inside the flow, thus enhancing the mechanical mixing capacity of the flow. However, if it is relatively easy to scale this improvement for a purely mechanical mixing, there is nothing in the polymer processing literature on the consequences of a change in a drag and pressure driven flow configuration when combined convection and diffusion physics are taking place.

Recognising that the flow profile is central to the laminar dispersion problem, which is close to the subject studied here, we envisage that changing the screw channel flow configuration will have profound repercussions also on the heat transfer taking place in this channel and that it is a matter of interest to investigate the forced convection heat transfer for a drag and pressure driven flow, in the same fashion as the forced convection heat transfer with pressure driven flows (Poiseuille flows) of Newtonian fluids [3, 5, 7, 14, 17] or non-Newtonian materials [4, 13, 18, 20] have been studied before.

In the first section, the flow features and relevant dimensionless numbers are established to set the framework for the forced convection heat transfer problem in a drag and pressure driven flow between parallel plates.

Polymer melts are shear-thinning fluids (power-law fluids) by opposition to constant viscosity fluids (Newtonian fluids). The major consequence of shear-thinning is on the pressure gradient which could be an order of magnitude smaller than its constant viscosity counterpart at the same flow rate. Nonetheless, this does not translate to the velocity profile. Indeed, when a drag driven flow velocity component is present, there are only minute differences between a shear thinning fluid drag and pressure driven flow profile and the equivalent constant viscosity flow profile, if an identical flow rate is prescribed [12, p. 118-122]. But both the analytic expression of the velocity profile and the search for the eigenvalues would be considerably more complex in the case of a drag and pressure driven power-law fluid flow.

As we are chiefly concerned with the influence of the velocity profile in this particular laminar dispersion problem, we set aside the simplifying hypothesis of a slug flow as in [2, 3, 6, 16], though slug flows will provide useful comparisons with our results.

Furthermore, owing to the large thermal capacitance of the metallic barrel wall operating at a steady regulated temperature we attempt no treatment of the conjugate heat transfer problem between the flow and its wall boundary [7] and will be only considering the isothermal case here.

Finally, for the purpose of clarity, we do not take into account the heat generation by viscous dissipation in the transient heat transfer part of this work. Instead, we limit ourselves to the study of viscous heating in the steady state heat transfer, because viscous heating acts as a non-homogeneous steady state heat source in the energy conservation equation. Nevertheless, the development presented here could be extended to the case where viscous

dissipation is present.

In the second section, the integral transform method used throughout this work is reviewed. The integral transform method is a well established analytic method in the field of forced convection heat transfer and has found numerous applications in steady state and transient heat transfer, particularly for heat exchangers [5, 6, 7, 8, 10, 14, 13, 16, 20] and recently in microfluidics [15, 17].

Integral transform gives a much clearer view on the structure of the solution in one or two dimensional convection-diffusion flows than any of the classical numerical methods like finite element, finite difference, or finite volume methods. A most appealing feature of this method is that it computes a very limited set of eigenvalues and associated eigenfunctions, unique to a given problem and does not require any space or time discretization procedure.

These eigenvalues reveal how the temperature, subject to convection and diffusion, propagates and dampen along the flow direction. Moreover, and most importantly, because these eigenvalues are tensorial scalars, they are invariant under coordinate transformations, hence they can be readily used to compare different types of flow unambiguously, and to establish objective mixing or dispersion criteria.

The integral transform method is applied to the transient energy conservation equation with the laminar velocity profile obtained for drag and pressure driven flows of a Newtonian fluid. First, the steady laminar forced convection heat transfer problem is solved and extended next to the transient case with a periodic single frequency transient inlet temperature. In this later part, we follow exactly the procedure established by Cotta and Özişik [5], in that we search for the periodic part of the transient problem solution.

In their seminal work [5] Cotta and Özişik did not solve the complex eigenvalue problem, this at the cost of producing a infinite system of coupled ordinary differential equations that has to be truncated to a finite number. Nevertheless, their procedure is extremely efficient and requires only a very limited number of complex eigenvalues to get entirely sufficient accuracy, as our validation with a Finite Element Method code will abundantly show in section four of this article. Moreover, the efficiency of their procedure is not limited to small transient frequency, but persists well above the low value investigated in their earlier work [5, 7]. We are able to report specific dampening effect of the inlet temperature disturbance at higher frequencies.

2. Heat transfer in a screw channel metering zone

2.1. Characteristic lengths, times and dimensionless numbers

A standard extrusion single screw metering channel is described in Tab. 1 together with the typical processing range and relevant polymer properties. It can be noticed that the screw channel in the metering zone is shallow, hence its curvature is small and its width is fifteen time larger than its depth. Therefore, the helical screw channel can be viewed as a rectangular duct of infinite width, hence as a parallel plate channel. Moreover, standard screws have a pitch equal to their diameter, implying that the screw angle is low and the unwound length is quite large as shown in Tab. 1.

The Brinkman number B_r is defined by the ratio between viscous heating and a characteristic temperature difference set by the process. When the polymer is expected to be completely molten such as in the metering zone of the screw channel, or in a extrusion die, no such prescribed temperature difference exists, and only viscous heating can be the source of a

Polymer properties			
Type	High Density Polyethylene		
Thermal diffusivity	D	$\approx 10^{-7}$ m^2/s	
Density	ρ	≈ 750 kg/m^3	
Thermal conductivity	k	≈ 0.2 W/m/K	
Viscosity	η	≈ 500 Pas	
Screw geometry			
Diameter	D_b	36 mm	
Pitch	P	36 mm	Angle 17°
Channel depth	H	2 mm	metering zone
Channel length	L	83 cm	unwound
Channel width	W	3cm	cross-channel
Curvature	$2H/D_b$	0.11	
Processing parameters			
Barrel Temperature	T_b	190°C	
Screw frequency	$\dot{r}$	30 rpm	100 rpm
Peripheral velocity	$V_{\mathrm{bz}} = Db\dot{r}/2$	5.4 cms^{-1}	18 cms^{-1}
Shear rate level	$\dot{\gamma} = V_{\mathrm{bz}}/H$	28 s^{-1}	94 s^{-1}
Viscous heating	$\Delta T = \eta V_{\mathrm{b}}^2/k$	7 °C	80 °C
Dimensionless numbers			
Reynolds	$R_e = \rho V_{\mathrm{b}} H/\eta$	$< 10^{-3}$	$< 10^{-3}$
Peclet	$P_e = HV_{\mathrm{b}}/D$	1080	3600
Graetz	$G_r = P_e H/L$	2.6	8.6
Brinkman	$B_r = \eta V_{\mathrm{b}}^2/(k\Delta T)$	1	1
Dimensionless screw frequency	Ω	125	420

Table 1: Typical polymer properties, screw channel geometry and processing parameters, together with the relevant dimensionless numbers encountered in polymer processing.

temperature difference. Therefore, we chose viscous heating as the characteristic temperature scale in Tab. 1 and consequently set the Brinkman number to one.

2.2. Drag and pressure driven velocity profile

The standard screw channel in the metering zone, as described in Tab. 1, can be modelled as a shallow rectangular duct of infinite width, with the barrel wall moving relative to the screw wall, hence reducing the complexity of a three-dimensional transient flow to a two dimensional parallel plate steady state flow [11], [12, p. 250]. Moreover, the Reynolds number should be very low for polymer melt flows, as shown in Tab. 1, with the consequence that the flow is laminar.

Selecting the channel depth in the metering zone as reference length H and the circumferential screw velocity V_{bz} as reference velocity, we have the drag and pressure driven dimensionless velocity profile :

$$u(y) = p_g(y^2 - y) + y \tag{1}$$

$$p_g = \frac{\Delta P}{L}\frac{H^2}{2\eta_0 V_{\mathrm{bz}}} \tag{2}$$

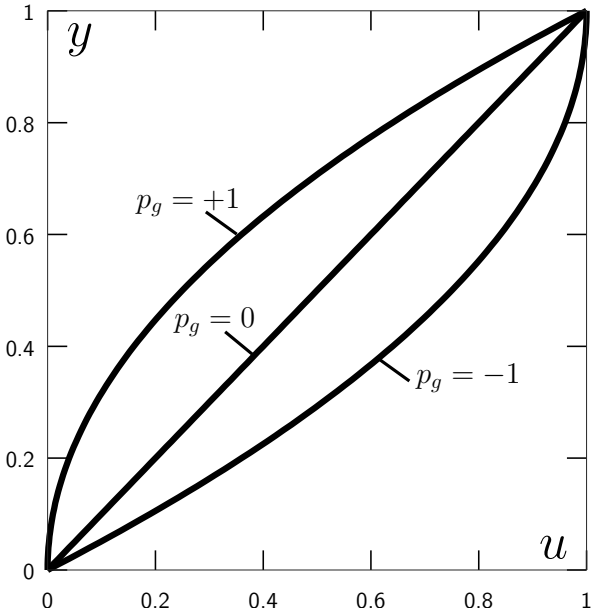

Figure 1: Velocity profiles $u(y)$ for different levels of pressure gradient $p_g : -1, 0, 1$ in drag and pressure driven flows

$$y = \frac{Y}{H} \tag{3}$$

where y is the dimensionless depth and p_g is a dimensionless pressure gradient which value can be selected at will, and which changes the flow configuration as seen in Fig. 1, η_0 a viscosity and ΔP a pressure difference. This dimensionless pressure gradient is built on the ratio between the actual pressure gradient and the shear stress in the channel.

We will limit ourselves in this study to pressure gradients not too large ($p_g \leq +1$) as to create a backflow, which would, in all rigour, require a three-dimensional flow analysis.

The advection-diffusion equation is used to describe the temperature evolution in the screw channel, as outlined in Eq. 4 the left term refers to the thermal advection in the flow direction z and the right term represents the thermal diffusion in the depth direction y :

$$\frac{\partial \theta}{\partial \tau} + u(y)\frac{\partial \theta}{\partial z} = \frac{\partial^2 \theta}{\partial y^2} \tag{4}$$

with :

$$z = \frac{DZ}{H^2 V_{\text{bz}}}, \quad \tau = \frac{Dt}{H^2}, \tag{5}$$

and homogeneous wall boundary conditions :

$$\begin{aligned} \theta(0, z, \tau) &= 0 \\ \theta(1, z, \tau) &= 0 \end{aligned}$$

In the preceding equations D is the thermal diffusion coefficient, z the dimensionless space variable in the flow direction and τ the dimensionless time. The Peclet number P_e usually

reaches value of 1000 or more, making the case for a convection dominated problem analysis, hence with the axial conduction term excluded from Eq. 4.

The inlet boundary condition at $z = 0$ is to be specified whether the problem is steady state in §3.1 or periodic in §3.3.

3. Integral transform method for forced convection heat transfer in parallel plate channels

3.1. Steady-state solution

The steady-state forced convection problem with homogeneous boundary conditions is viewed as a class I problem in the classification given by Mikhailov [9].

$$u(y)\frac{\partial\theta}{\partial z} = \frac{\partial^2\theta}{\partial y^2} \tag{6}$$

$$\mu_k^2 u(y) Y_k + \frac{d^2 Y_k}{dy^2} = 0 \tag{7}$$

$$Y_k = 0 \text{ at } y = 0 \text{ and } y = 1 \tag{8}$$

where finding the temperature field $\theta(y, z)$ is the main problem and finding the eigenvalues μ_k and the corresponding eigenfunctions $Y_k(y)$ with homogeneous boundary conditions is the auxiliary problem. The customary integral transform pair is therefore defined as :

$$\bar{\theta}_k(z) = \int_0^1 \frac{1}{N_k} u(y)\theta(y,z)Y_k(y)dy \tag{9}$$

$$\theta(y,z) = \sum_{k=1}^{\infty} \frac{1}{N_k}\bar{\theta}_k Y_k(y) \tag{10}$$

$$N_k^2 = \int_0^1 u(y)Y_k(y)Y_k(y)dy \tag{11}$$

where N_k is the norm of the eigenfunction.

The inlet boundary condition at $z = 0$ could be be any function of y :

$$\theta(y, 0) = f(y) \tag{12}$$

The integral transform of the temperature field obeys the ordinary differential equation :

$$\frac{d\bar{\theta}_k}{dz} + \mu_k^2\bar{\theta}_k = 0 \tag{13}$$

which readily admits the solution :

$$\bar{\theta}_k = \bar{f}_k \exp\left(-\mu_k^2 z\right) \tag{14}$$

where $\bar{f}_k$ is the integral transform of the inlet boundary condition Eq. 12.

Compounding calculations above, we can express the temperature field solution as

$$\theta(y,z) = \sum_{k=1}^{\infty} \frac{1}{N_k}\bar{f}_k \exp\left(-\mu_k^2 z\right) Y_k(y) \tag{15}$$

3.2. Viscous dissipation

In the case of shear flows, the viscous dissipation will act as a steady state non-homogeneous heat source to be added to the RHS of Eq. 6:

$$B_r \left(\frac{\partial u}{\partial y} \right)^2 \tag{16}$$

where B_r is the Brinkman number scaling the viscous heating and $\frac{\partial u}{\partial y}$ is the steady state shear rate field. A fully developed developed temperature θ_∞ can then be computed from the balance between heat conduction and viscous dissipation in Eq. 6 as:

$$\theta_\infty(y) = B_r \left(\frac{p_g^2}{3}(y - y^4) - \frac{2}{3} p_g (p_g - 1)(y - y^3) + \frac{1}{2}(p_g - 1)^2 (y^2 - y) \right) \tag{17}$$

Next, a split of the temperature field $\theta_{\text{vh}}(y, z)$ between the steady state part $\theta(y, z)$ and the fully developed part $\theta_\infty(y)$

$$\theta_{\text{vh}}(y, z) = \theta_(y, z) + \theta_\infty(y) \tag{18}$$

will lead to the inlet boundary condition at $z = 0$:

$$f(y) = -\theta_\infty(y) \tag{19}$$

The integral transform can then be performed as described in §3.1 to solve for the $\theta(y, z)$ part.

3.3. Transient solution

The transient heat transfer problem is defined in Eq. 20.

$$\frac{\partial \theta}{\partial \tau} + u(y) \frac{\partial \theta}{\partial z} = \frac{\partial^2 \theta}{\partial y^2} \tag{20}$$

$$\theta(0, z, \tau) = 0 \tag{21}$$

$$\theta(1, z, \tau) = 0 \tag{22}$$

$$\theta(y, 0, \tau) = \cos(\Omega \tau) \tag{23}$$

where the same thermal boundary conditions apply as before except for the inlet temperature which is now periodic. Cotta's work states that a periodic solution is to be found as the real part of the following complex solution :

$$\theta(y, z, \tau) = \text{Re} \left(\tilde{\theta}(y, z) \exp(i \Omega \tau) \right) \tag{24}$$

The unknown temperature field $\tilde{\theta}$ is put into the previous differential equation Eq. 20 to form a new set of problems :

$$i \Omega \tilde{\theta} + u(y) \frac{\partial \tilde{\theta}}{\partial z} = \frac{\partial^2 \tilde{\theta}}{\partial y^2} \tag{25}$$

while keeping the same auxiliary problem given in Eq. 7. This departs from the classic Integral Transform Method, but avoids having to solve a eigenvalue problem in the complex space.

The integral transform pair is now defined as :

$$\bar{\tilde{\theta}}_j(z) = \int_0^1 \frac{1}{N_j} u(y) Y_j(y) \tilde{\theta}(y,z) dy \tag{26}$$

$$\tilde{\theta}(y,z) = \sum_{j=1}^{\infty} \frac{1}{N_j} Y_j(y) \bar{\tilde{\theta}}_j(z) \tag{27}$$

Following the integral transform method, the integral of the partial differential equations Eq. 25 and Eq. 7 are performed over the interval $y = [0,1]$. Integrating by part the second derivatives in each equations, an infinite linear set of coupled ordinary differentials equations is obtained :

$$\frac{d\bar{\tilde{\theta}}_k}{dz} = -\mu_k^2 \bar{\tilde{\theta}}_k - i\Omega \sum_{j=1}^{\infty} b_{kj} \bar{\tilde{\theta}}_j \tag{28}$$

$$b_{kj} = \frac{1}{N_k N j} \int_0^1 Y_j Y_k dy \tag{29}$$

This system of coupled differential equations has to be truncated to the same number of computed eigenvalues in order to be solved in practice. Introducing the vector X of unknown transformed temperature

$$\underline{X}(z) = \left(\bar{\tilde{\theta}}_1(z), \ldots, \bar{\tilde{\theta}}_k(z), \ldots, \bar{\tilde{\theta}}_N(z) \right) \tag{30}$$

The vector $\underline{X}$ is now the solution of a symmetric finite linear set of differential equations :

$$\dot{\underline{X}} = -\underline{\underline{A}} \cdot \underline{X} \tag{31}$$

$$= -\left(\underline{\mu}^2 \cdot \underline{\underline{1}} + i\Omega \underline{\underline{B}} \right) \tag{32}$$

$$A_{kj} = \mu_k^2 \delta_{kj} + i\Omega B_{kj} \tag{33}$$

with the real positive eigenvalues μ_k^2 positioned on the diagonal of the complex matrix $\underline{\underline{A}}$. Cotta and Özişik [5] chose to solve this system by computing the eigenvalues λ_k and eigenvectors $\underline{v}^k$ of $\underline{\underline{A}}$. Hence, the solutions vector $\underline{X}$ is expressed in the eigenvectors basis as :

$$\underline{X}(z) = \sum_{k=1}^{N} C_k \exp\left(-\lambda_k z\right) \underline{v}^k \tag{34}$$

where the coefficient C_k can be found by expressing the initial condition vector $\underline{x}(0)$ in the eigenvectors basis also.

4. Results and discussion

4.1. Eigenvalues and eigenfunctions calculation

The eigenvalue problem described in Eq. 7 and Eq. 8 is solved in a straightforward fashion following the procedure described by [1]. The unknown eigenfunction is expanded in a series of increasing power of the variable y :

$$Y_k(y) = \sum_{i=1}^{i=251} b_{ki} y^i \tag{35}$$

drag and pressure driven flow				slug flow		
p_g	-1	0	1			$\pi/\sqrt{\langle u \rangle}$
$\langle u \rangle$	2/3	1/2	1/3	2/3	1/2	1/3
μ_1	3.6723	4.35388	5.5618	3.8476	4.4429	5.4414
μ_2	7.6688	9.04912	11.8123	7.6953	8.8858	10.8828
μ_3	11.6679	13.7558	18.0848	11.5429	13.3286	16.3342
μ_4	15.6675	18.4653	24.3627	15.3906	17.7715	21.7756
μ_5	19.6673	23.1760	30.6427	19.2382	22.2144	27.2270
μ_6	23.6671	27.8872	36.9239	23.0853	26.6573	32.6484
μ_7	27.6670	32.5988	43.2056	26.9335	31.1002	38.0898
$\Delta\mu_{k,k+1}$	4	4.71	6.28	3.85	4.44	5.44

Table 2: First seven eigenvalues computed for the three different cases of pressure gradient p_g and corresponding average dimensionless velocity $\langle u \rangle$. Comparison with the slug flow with same average velocity $\langle u \rangle$.

where b_{ki} are unknown coefficients to be determined by a recurrence relation. This recurrence relation is readily established by applying the differential equation to the polynomial expression of Y_k in Eq. 35. The choice to express the eigenfunctions as polynomials is apt because the velocity profile $u(y)$ is itself a polynomial. Finally, the homogeneous boundary condition at $y = 1$ is used as a non linear equation of which the eigenvalues μ_k are the roots of.

It is worth recalling that a particular eigenvalue problem is attached to a velocity profile defined in Eq. 1 by the chosen value of the parameter p_g. In this work, three different values of p_g are chosen to be representative of the different flow configurations : $p_g = 0$ for pure drag flow, $p_g = -1$ for pressure loss and drag flow, and $p_g = 1$ for backpressure flow as seen in Fig.1.

In Tab. 2 the first seven eigenvalues are given : It can be seen that these eigenvalues tend to be evenly spaced, with the average difference between two consecutive eigenvalues given in the last line of Tab. 2. Checking the accuracy of the procedure can be performed by inserting the computed eigenfunctions back into the auxiliary problem Eq. 7 and plotting the residual along the variable y in Fig. 2, right. It can be seen that the error remains below 10^{-6} at most, for the largest computed eigenvalue. The corresponding eigenfunctions are drawn in Fig. 2 for a pressure gradient $p_g = +1$.

4.2. Steady state temperature solution

The increasing temperature due to viscous heating along the flow direction is displayed Fig. 3 for the three different pressure gradients $pg = -1, 0, +1$. Although the amount of self heating is similar across the cases, the temperature is much closer to the fully developed temperature profile when a positive pressure gradient is applied ($p_g = +1$). The comparison between the model computed with seven eigenvalues and the FEM simulation results is very good, even at short length ($z = 0.01$).

4.3. Periodic temperature solution

The most important question this model was built to answer is how an inlet temperature fluctuation with a given frequency Ω is transported at the other end of the screw channel, how this signal is distorted and to what extent its amplitude and phase lag are affected by the particular velocity profile in use. A straightforward mean to assess this is to follow the

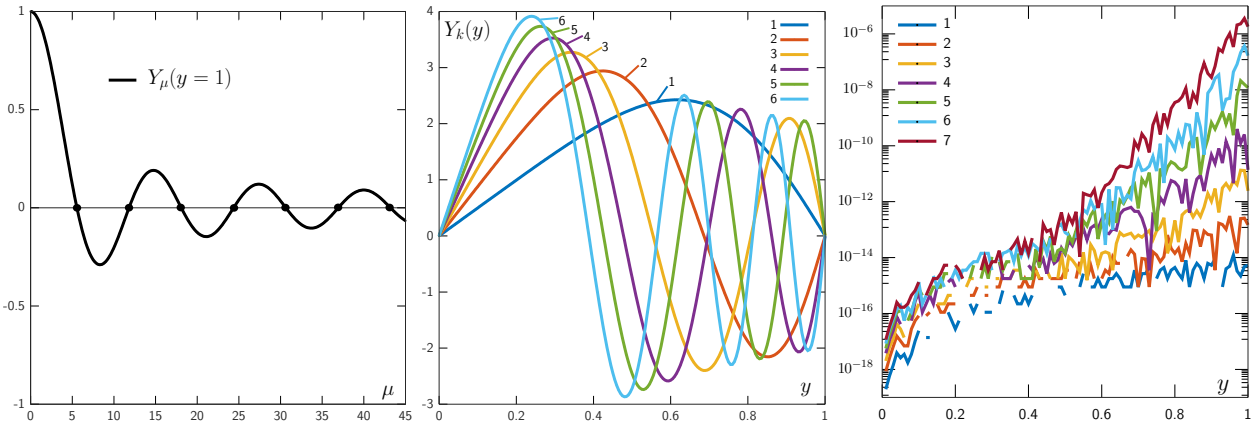

Figure 2: Computation of eigenvalues and eigenfunctions in the case of pressure gradient $p_g = +1$: Location of the eigenvalues, left; Plot of the six first eigenfunctions, centre; Residual of the auxiliary problem along y for each eigenfunction, right.

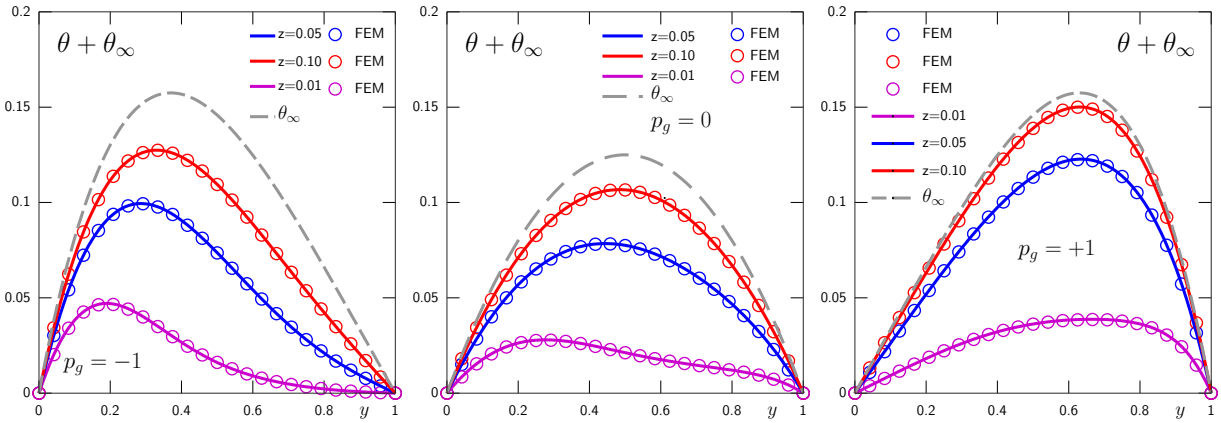

Figure 3: Temperature profiles along dimensionless channel depth y at locations $z = 0.01, 0.05, 0.10$, for three different dimensionless pressure gradients $p_g = -1, 0, +1$. Steady state heat transfer with viscous dissipation $B_r = 1$. Integral transform model predictions (solid lines) and FEM simulation results (circles)

temperature over time at a given location downstream from the inlet boundary. This is also called a breakthrough curve when one refers to a mass transfer problem. Therefore, we define the mixing cup average temperature and the length average temperature over the channel depth as :

$$\theta_{\mathrm{mxcp}}(z,\tau) = \frac{1}{q}\int_0^1 u(y)\theta(y,z,\tau)dy \tag{36}$$

$$\theta_{\mathrm{lav}}(z,\tau) = \int_0^1 \theta(y,z,\tau)dy \tag{37}$$

where q is the dimensionless flow rate.

4.3.1. Model validation

Comparisons between the mixing cup average temperature computed from the model and from Finite Element Method (FEM) simulation results are shown in Fig. 5 at two different locations $z = 0.05, 0.1$ for the three different levels of pressure difference $p_g = -1, 0, +1$ and three different dimensionless frequencies $\Omega = 5$, 10, 50. The fully transient FEM simulations were carried out with $P_e = 1000$ and with axial conduction taken into account in the energy conservation equation.

The mesh used was 48X400 quadrilateral elements, equally spaced along the channel depth and length for all cases. Calculations at the largest inlet temperature frequency $\Omega = 50$ where performed once more with a refined mesh 96X800. This led to a maximum relative variation of 0.11% between the results, but at a prohibitive computational cost. The Crank Nicolson's time marching scheme was chosen with a maximum time step $d\tau = 8.10^{-4}$.

4.3.2. Model convergence

Although the accuracy of the model computed will look very good in Fig. 5, we need to assess more precisely the precision level reached by the integral transform method solution with the number of eigenvalues employed, by comparing this solution to the FEM simulation results.

Tab. 3 displays the values of the mixing cup average temperature at two different locations, for three inlet frequencies and three pressure gradients. For all cases, with the exception of the positive pressure gradient $p_g = +1$ at the highest dimensionless inlet frequency $\Omega = 50$, the absolute error between the FEM results and the model is at most 6.0e-4, this amounts to being in agreement to at least three digits in value.

Plotting the relative error between the model and the FEM simulation results against the number N of eigenvalues used to compute the model gives a clearer sense of the convergence across the cases Fig. 4. It emerges that the precision degrades with increasing pressure gradient p_g and increasing inlet frequency Ω. The lowest relative error is obtained for $p_g = -1$ and $\Omega = 5$, whereas the largest relative error is encountered for $p_g = +1$ and $\Omega = 50$. It should be pointed out that in this particular case the amplitude of the inlet temperature perturbation has been divided by one thousand. This doubtless explains why the mismatch between the model and the FEM simulation results is at its largest there. Moreover, for the lower relative error cases there is no much improvement when using more eigenvalues, whereas for the highest error case there is a two decades improvement in accuracy from computations with one eigenvalue to seven eigenvalues.

p_g	Ω	τ	z	$\theta_{\text{mxcp}}(z,\tau)$					$\Delta\theta_{\text{mxcp}}$
				$N=1$	$N=3$	$N=5$	$N=7$	FEM	$N7-$FEM
-1	5	2.0	0.05	-0.4184	-0.4178	-0.4178	-0.4178	-0.4172	-6.2e-04
-1	5	2.0	0.10	-0.2185	-0.2175	-0.2175	-0.2174	-0.2171	-3.2e-04
-1	10	1.5	0.05	-0.08237	-0.08368	-0.08361	-0.08358	-0.08345	-1.3e-04
-1	10	1.5	0.10	0.1009	0.09788	0.09778	0.09776	0.0976	1.6e-04
-1	50	0.5	0.05	-0.4056	-0.3417	-0.3417	-0.3418	-0.3414	-3.8e-04
-1	50	0.5	0.10	0.1867	0.1286	0.1302	0.1305	0.1305	3.3e-05
0	5	2.0	0.05	-0.3197	-0.3178	-0.3177	-0.3177	-0.3175	-1.6e-04
0	5	2.0	0.10	-0.1172	-0.1159	-0.1159	-0.1159	-0.1158	-5.0e-05
0	10	1.5	0.05	0.01973	0.01438	0.01424	0.01423	0.01419	3.5e-05
0	10	1.5	0.10	0.104	0.09711	0.09686	0.09682	0.09674	7.6e-05
0	50	0.5	0.05	0.0133	-0.04501	-0.05033	-0.05101	-0.05132	3.1e-04
0	50	0.5	0.10	-0.1246	-0.0264	-0.02711	-0.02724	-0.02728	3.6e-05
$+1$	5	2.0	0.05	-0.172	-0.1681	-0.1678	-0.1677	-0.1675	-2.3e-04
$+1$	5	2.0	0.10	-0.02499	-0.02421	-0.02417	-0.02416	-0.02413	-2.4e-05
$+1$	10	1.5	0.05	0.08904	0.07349	0.07229	0.07201	0.07168	3.3e-04
$+1$	10	1.5	0.10	0.03441	0.02821	0.02798	0.02793	0.02787	5.7e-05
$+1$	50	0.75	0.05	0.104	0.02854	0.03292	0.03382	0.03434	7.0e-02
$+1$	50	0.75	0.10	-0.003112	-0.0004224	-0.0002405	-0.0001793	-0.0001326	-3.0e-03

Table 3: Mixing cup average temperature values $\theta_{\text{mxcp}}(z,\tau)$ computed from integral transform model with varying number of eigenvalues $N = 1, 3, 5, 7$, and FEM results for the three different pressure gradients $p_g = -1, 0, +1$ and three different inlet disturbance frequencies $\Omega = 5, 10, 50$, at two different locations $z = 0.05, 0.10$. Last column: Absolute error between mixing cup average temperature at $N = 7$ and FEM simulation results.

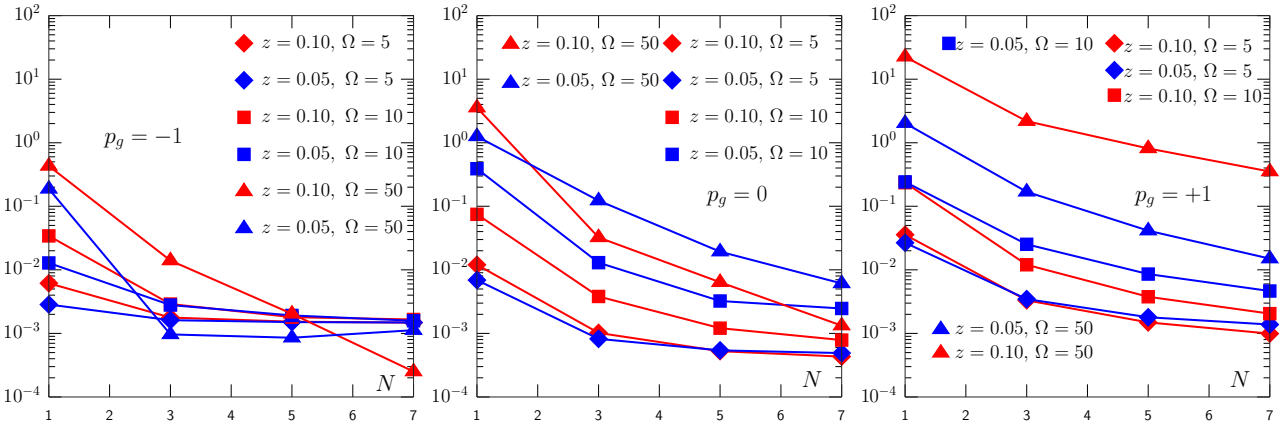

Figure 4: Relative error of mixing cup average temperature $\theta_{\text{mxcp}}(z,\tau)$ between the integral transform model and FEM simulations results along number of eigenvalues N, for the three different pressure gradients ($p_g = -1, 0, +1$ and three different inlet disturbance frequencies $\Omega = 5, 10, 50$, at two different locations $z = 0.05, 0.10$

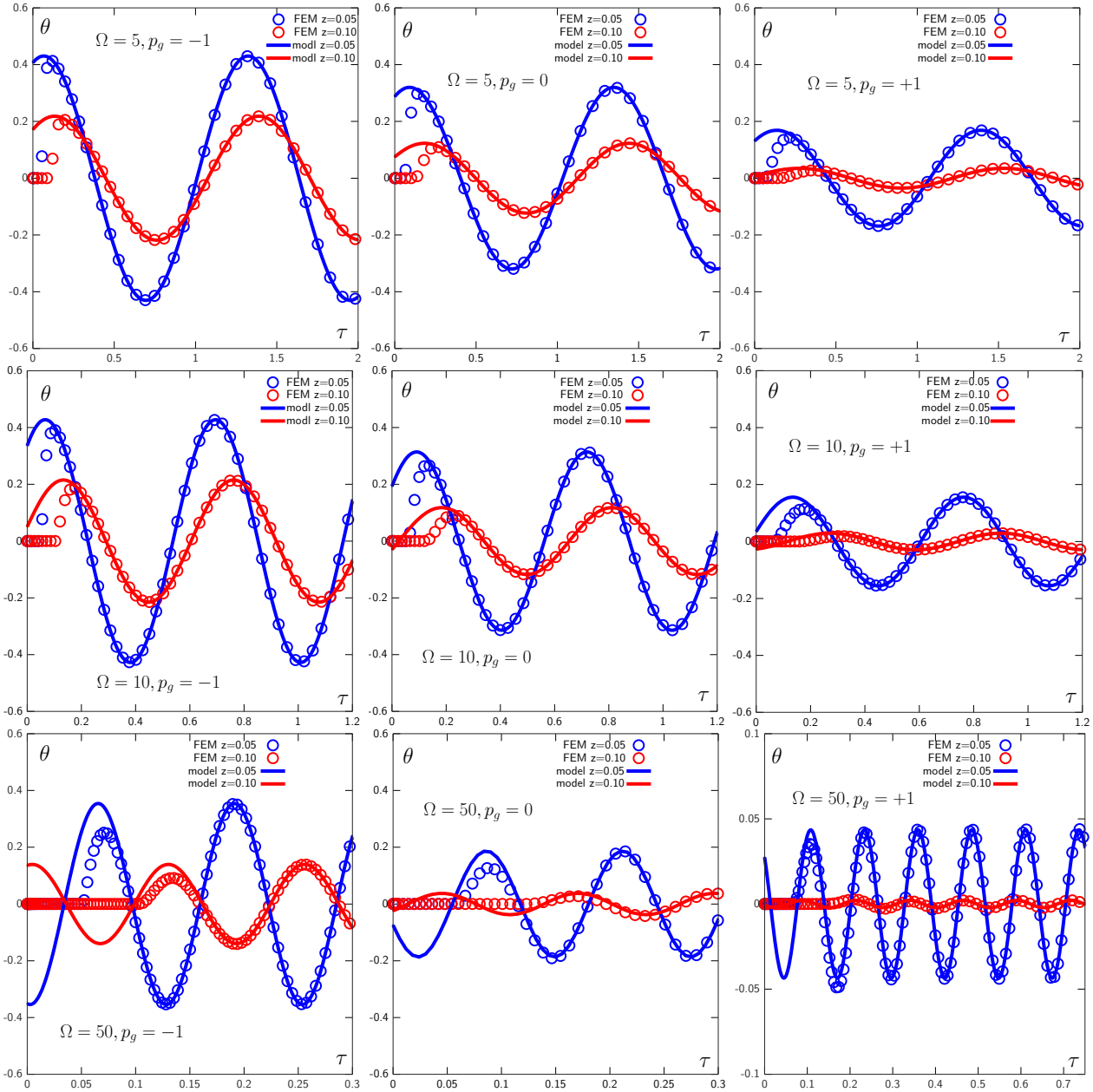

Figure 5: Mixing cup average temperature along dimensionless time τ for the three different value of dimensionless pressure gradient : $p_g = -1$ left column ; $p_g = 0$, centre column; $p_g = +1$, right column. Inlet temperature frequency $\Omega = 5$, top row; $\Omega = 10$, centre row, $\Omega = 50$, bottom row. Comparison between model predictions (solid blue line $z = 0.05$, solid red line $z = 0.1$) and FEM simulation results (circle) at $P_e = 1000$.

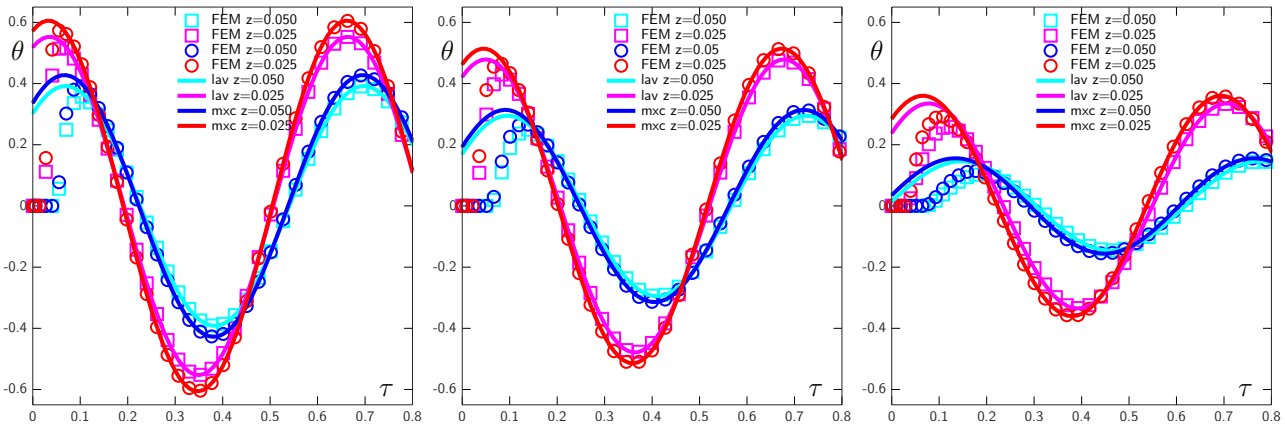

Figure 6: Length average ("lav") and mixing cup ("mxc") average temperatures along dimensionless time τ at locations $z = 0.025$ and $z = 0.05$ for the three different values of dimensionless pressure gradient : $p_g = -1$ left; $p_g = 0$, centre; $p_g = +1$, right. Comparison between model predictions and FEM simulation results at $P_e = 1000$. Inlet temperature frequency $\Omega = 10$.

4.3.3. Breakthrough curves of average temperature

A number of insights can be obtained from the results Fig.5 and Fig.6. First, once the temperature wave has reached the chosen location in the screw channel, it can be seen that the match between the periodic solution given by the model and the fully transient FEM solution is perfect, at longer time, whether for the amplitude or the phase, for all inlet temperature frequencies ($\Omega = 5$, 10, 50) and for all pressure gradients ($p_g = -1$, 0, $+1$). Let us remind that the model gives the periodic solution, valid at the longer timescale, whereas the FEM simulation is fully transient and gives both the transient and the periodic solution.

The case of the backpressure flow $p_g = +1$ with inlet temperature frequency $\Omega = 50$ in Fig. 5 is particularly interesting: In the FEM simulation results, once the temperature wave has reached the location at $z = 0.1$, the transient temperature exhibits first an amplitude undershoot, followed by an overshoot and then matches the periodic solution at longer time.

The accuracy of the temperature solution given by the integral transform model is on display again in Fig. 6 where the comparison between the mixing cup, length averaged temperature and FEM simulation results are plotted. Because the velocity profiles differs from a slug flow, there are differences between the mixing cup and the length averaged temperatures, though they are quite small. Nevertheless, there is still a perfect match between each type of average temperature and the corresponding FEM calculations.

This validates completely Cotta and Özişik's approach but here for a larger dimensionless frequency Ω and for a different velocity profile from the pressure driven flow they considered in [5] for instance.

Second, we can clearly see in Fig. 5 the extent of the dampening of the inlet temperature signal when a higher backpressure is employed. The higher the backpressure p_g, the higher the amplitude dampening of the inlet temperature.

Turning now to the effect of the inlet disturbance frequency on the temperature field, it is of interest to notice in Fig. 5 that a larger dampening of the temperature signal is observed when a higher frequency Ω is considered.

This has, to our best knowledge, never been reported in the literature [5, 2, 7, 3, 10] before,

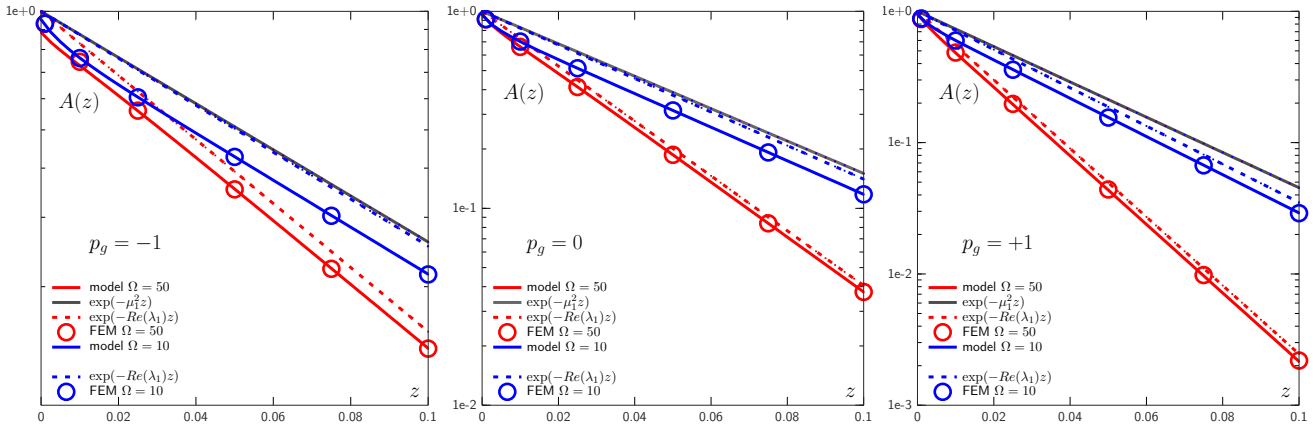

Figure 7: Amplitude of mixing cup average temperature (solid line) along dimensionless space z, at dimensionless pressure gradient $p_g = -1$ left; $p_g = 0$, centre; $p_g = +1$, right, at dimensionless frequency $\Omega = 10$ (blue colour) and $\Omega = 50$ (red colour). Comparison between model (solid blue or red lines) and exponential dampening with μ_1^2 (solid gray line) and $\mathrm{Re}(\lambda_1)$ (dashed blue or red line) factors, and FEM simulation results at $P_e = 1000$ (circle).

because the frequencies these authors considered where smaller than those we considered here.

4.3.4. Amplitude and phase lag

We recast the mixing cup average of the complex temperature solution $\tilde{\theta}_{\mathrm{mxcp}}$ as :

$$\tilde{\theta}_{\mathrm{mxcp}} = A(z) \exp\left(i\Omega\tau + \phi(z)\right) \tag{38}$$

where $A(z)$ and $\phi(z)$ stand for the amplitude and the phase lag of the periodic temperature solution.

The evolution of the mixing cup average temperature amplitude along z, given both by the model and the FEM simulation results, are displayed in Fig. 7. The temperature decay is very well predicted by the model, up to nearly three decades in magnitude in the case of $p_g = +1$ and $\Omega = 50$, as proved by the match with the FEM simulation results. Only seven eigenvalues were needed to get to this level of accuracy.

Inspection of the differential equations system in matrix form Eq. 32 and Eq. 34 suggests that the amplitude $A(z)$ should scale with the real part of the lowest complex matrix eigenvalue λ_1, whereas the phase lag $\phi(z)$ should scale with its imaginary part. This is indeed the case for the amplitude plotted on Fig. 7 where the exponential dampening is obvious in the semi-logarithmic plot scale. Also undoubtedly clear is the fact that the long range behaviour of the amplitude is given by the real part of eigenvalue λ_1s and follows the relation:

$$A(z) = A_0 \exp\left(-\mathrm{Re}(\lambda_1)z\right) \tag{39}$$

When the frequency Ω is small, the eigenvalue λ_1 does not differ much from its steady-state real counterpart μ_1^2, because the complex part of the solution scales with Ω.

The evolution of the phase lag normalised by the frequency Ω along the flow direction z is plotted on Fig. 8 for the three different pressure gradients $p_g = -1, 0, +1$ and for two different dimensionless frequencies $\Omega = 5, 50$. The phase lag evolution is linear with z, showing a continuously increasing delay between the inlet temperature signal and its measurement at any point z.

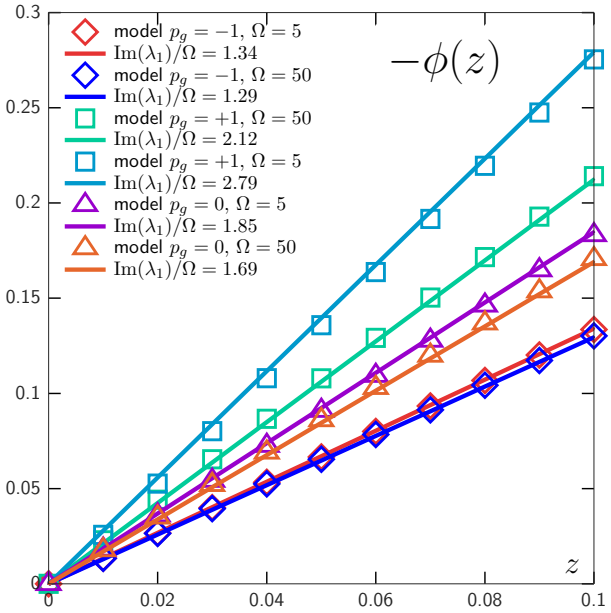

Figure 8: Evolution of phase lag of the mixing cup average temperature $\phi(z)$ along flow direction z. Values are normalised by inlet temperature dimensionless frequency Ω. Comparison between model solution (symbols) and linear relation (solid lines) Eq. 40.

The phase lag is much larger when a positive pressure difference (backpressure) is used as evidenced by the results for $p_g = +1$ in Fig. 8.

Moreover, in all cases this linear evolution is well captured by the linear relation :

$$\phi(z) = -\mathrm{Im}(\lambda_1)\Omega z \tag{40}$$

However, the imaginary part of the lowest eigenvalue λ_1 depends itself on Ω as indicated by the difference of slopes between the cases at $\Omega = 5$ and $\Omega = 50$ for the flow with pressure gradient $p_g = +1$.

4.3.5. Effect of velocity profile

We have previously stated that by increasing the pressure gradient towards positive values (backpressure), while keeping the drag velocity constant, the dispersion of the inlet temperature disturbance will be much more efficient. Changing the backpressure setting while keeping the same screw frequency is indeed common practice in the polymer processing industry. However, this is at the cost of lowering the average velocity of the flow, or equivalently increasing the residence time and allowing more time for diffusion. Thus the better dispersion of the inlet temperature disturbance when increasing the backpressure should not come as a surprise.

If we wish to close in on the effect of velocity profile solely, we should compare the temperature solution at the same average velocity for different pressure gradients.

In the steady state heat transfer case, the solution Eq. 14 implies that the evolution of temperature is governed by the exponential of the successive eigenvalues μ_k^2. Precisely, if we convert the variable z from a Peclet number P_e based on drag velocity to a Peclet number P_{em} based on average velocity $\langle V \rangle$ we have :

$$-\mu_k^2 z \quad = \quad -\mu_k^2 \frac{1}{P_e} \frac{Z}{H}$$

drag and pressure driven flow				slug flow
p_g	-1	0	+1	
$\langle u \rangle$	2/3	1/2	1/3	
μ_1	3.67	4.35	5.56	$\mu_1 = \pi/\sqrt{\langle u \rangle}$
$\mu_1^2 \langle u \rangle$	9	9.47	10.31	9.87

Table 4: Comparison between the lowest eigenvalues for the three different pressure gradients p_g and the slug flow at the same average velocity $\langle u \rangle$

$$
\begin{aligned}
&= -\mu_k^2 \frac{P_{em}}{P_e} \frac{1}{P_{em}} \frac{Z}{H} \\
&= -\mu_k^2 \frac{\langle V \rangle}{V_{bz}} \frac{1}{P_{em}} \frac{Z}{H} \\
&= -\mu_k^2 \langle u \rangle \frac{Z}{H}
\end{aligned}
$$

where $\langle u \rangle$ is the dimensionless average velocity.

Thus, a valid comparison can be made between different velocity profiles at the same residence time by keeping constant both the Peclet number P_{em} and the location Z/H, hence computing the product $\mu_1^2 \langle u \rangle$. This results now Tab. 4 in a much more narrow distribution of values between a pressure drop, a drag and a backpressure flow. Still, the backpressure flow is characterised by a higher first eigenvalue, resulting in a better dispersing capacity than the other two flow configurations and to the equivalent slug flow.

For the periodic heat transfer case, we can compare the drag and pressure driven flow temperature solution to the slug flow temperature solution at the same average velocity (same residence time) in Fig. 9. Interestingly enough, at low frequency Ω, the pressure drop and drag flow are not really better at dispersing the inlet temperature disturbance than the equivalent slug flow, whereas the backpressure is improving upon the slug flow. However, at higher frequencies only the drag and backpressure flow show better dispersing capabilities than the slug flow. Indeed, slug flow dampening does not change with frequency Ω. This finding casts doubts on the relevance of the slug flow assumption to represent forced convection heat transfer in ducts [2, 3, 6, 16].

5. Conclusions

The integral transform method has been successfully used for forced convective heat transfer with transient inlet temperature for the drag and pressure driven flow in a single screw parallel plate channel.

The periodic temperature solution has been entirely checked against FEM simulation results for three different inlet temperature frequencies and three different values of the pressure gradient in the drag and pressure driven velocity profile that characterises the laminar flow in the metering zone of a polymer processing single screw.

The calculation procedure outlined by Cotta and Özişik [5] is fast and requires only a very limited number of eigenvalues to reach a very good accuracy, both in the case of low and high inlet temperature frequency.

Furthermore, the lowest eigenvalue contains all necessary information to characterise the long range evolution of the periodic temperature solution. This eigenvalue allows to compare

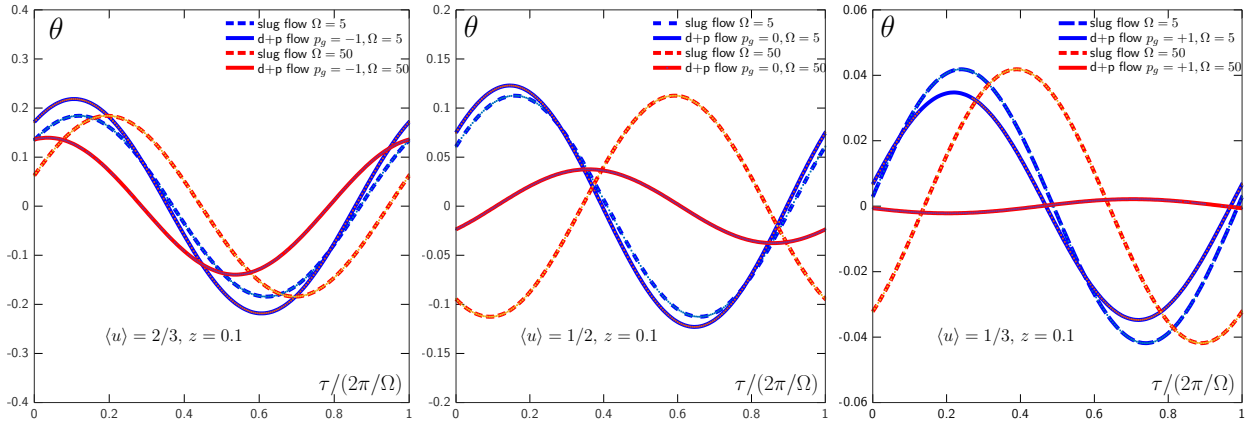

Figure 9: Mixing cup average temperature along dimensionless time τ at two different frequencies $\Omega = 5, 50$, at $z = 0.1$. Comparison between model predictions for drag and pressure driven flows ("d+p") for three different values of dimensionless pressure gradient $p_g = -1, 0, +1$ with the corresponding slug flow $\langle u \rangle = 2/3,\ 1/2,\ 1/3$.

unambiguously between drag and pressure driven flows with different pressure gradients, and also with slug flows at the same average velocities. Both the amplitude and the phase lag have been quantitatively related to the lowest complex matrix eigenvalue of the integral transform problem. Moreover, there is a large influence of the inlet temperature frequency on the amplitude dampening of the temperature wave and a linear dependence on its phase lag.

We conjecture that the systematic inclusion of a parameterised velocity profile into the auxiliary problem, though it forces to solve numerically a specific eigenvalue problem for each value of the parameter, is key to the fast convergence of the integral transform method in so few eigenvalues.

From the polymer processing stand point, the most important result is that a higher level of backpressure (positive pressure gradient) in the flow will result in a much more efficient dampening of the inlet temperature fluctuation, at the cost of a longer residence time or longer cycle time. If a constant cycle time is required, a higher backpressure is still improving on the dispersion of the inlet temperature disturbance but the improvement is lesser.

As far as the process stability is concerned, which was our prior motivation, this study demonstrates that only low frequency inlet temperature disturbances are to be scrutinised because higher frequency disturbances will be dampened very efficiently if some level of back-pressure is applied to the screw channel flow.

Lower frequency disturbances could come from the operation of the barrel heater band, upstream of the region of interest. It is customary that this system is allowed to vary around the prescribed temperature within a margin of $\pm 5°$C. For higher frequencies, one would speculate that the rotating screw could present a region of higher temperature, at the top of one flight for instance, perhaps because of lower clearance between the flight top and the barrel. In this case, the disturbance frequencies will be the dimensionless screw frequencies Tab. 1, which are even larger than those envisaged here. In any case, these very large frequency disturbances would have been wiped out by the end of the metering zone screw channel.

To further advance this study in the scope of polymer processing, we plan to include into the periodic solution both wall temperature disturbance and variations of the channel depth

that feature in the compression zone of a single screw.

Finally, it did occur to us that complex eigenvalues computed by the integral transform method for this periodic heat transfer problem could be linked to the complex eigenvalues sought for in a linear stability of an arbitrary transient perturbation. In further work we would like to see if the integral transform method could provide a more efficient tool than pseudo-spectral methods to solve for the eigenspectrum in the viscoelastic linear stability problem [19].

Acknowledgements

Support from FUI-AAP21 SAPRISTI Project is gratefully acknowledged for Y. Agbessi's postdoctoral fellowship. Support from China Scholarship Council is gratefully acknowledged for L. X. Bu's PhD grant.

References

[1] G. M. Brown. Heat or mass transfer in a fluid in laminar flow in a circular or flat conduit. *AIChE Journal*, 6(2):179–183, 1960.

[2] E.M. Sparrow and F.N. De Farias. Unsteady heat transfer in ducts with time-varying inlet temperature and participating walls. *International Journal of Heat and Mass Transfer*, 11(5):837 – 853, 1968.

[3] S. Kakaç and Y. Yener. Exact solution of the transient forced convection energy equation for timewise variation of inlet temperature. *International Journal of Heat and Mass Transfer*, 16(12):2205 – 2214, 1973.

[4] R. M. Cotta and M. N. Ozisik. Laminar forced convection of power-law non-newtonian fluids inside ducts. *Wärme and Stoffübertragung*, 20:211–218, 1986.

[5] R.M. Cotta and M.N. Ozisik. Laminar forced convection inside ducts with periodic variation of inlet temperature. *International Journal of Heat and Mass Transfer*, 29(10):1495 – 1501, 1986.

[6] R. M. Cotta, M. D. Mikhailov, and M. N. Ozisik. Transient conjugated forced convection in ducts with periodically varying inlet temperature. *International Journal of Heat and Mass Transfer*, 30(10):2073–2082, 1987.

[7] S. Kakac, W. Li, and R. M. Cotta. Unsteady laminar forced convection in ducts with periodic variation of inlet temperature. *Journal of Heat Transfer*, 112(4):913–920, 1990.

[8] R. Guedes and R. M. Cotta. Periodic laminar forced-convection within ducts including wall heat-conduction effects. *International Journal of Engineering Science*, 29(5):535–547, 1991.

[9] M. D. Mikhailov and M. N. Ozisik. *Unified analysis and solutions of heat and mass diffusion*. Dover, 1994.

[10] S Cheroto, MD Mikhailov, S Kakac, and RM Cotta. Periodic laminar forced convection: solution via symbolic computation and integral transforms. *International journal of thermal sciences*, 38(7):613–621, Jul-Aug 1999.

[11] Y. Béreaux, M. Moguedet, X. Raoul, JY. Charmeau, J. Balcaen, and D. Graebling. Series solutions for viscous and viscoelastic fluids flow in the helical rectangular channel of an extruder screw. *Journal of Non-Newtonian Fluid Mechanics*, 123(2-3):237–257, 2004. 10.1016/j.jnnfm.2004.08.011.

[12] Z. Tadmor and C. G. Gogos. *Principles of Polymer Processing*. John Wiley, 2004.

[13] Cassio Roberto Macedo Maia, João Batista Aparecido, and Luiz Fernando Milanez. Heat transfer in laminar flow of non-newtonian fluids in ducts of elliptical section. *International Journal of Thermal Sciences*, 45(11):1066 – 1072, 2006.

[14] G.E. Cossali. Analytical solution of graetz problem in pipe flow with periodic inlet temperature variation. *International Journal of Heat and Mass Transfer*, 52(13):3396 – 3401, 2009.

[15] L.A. Sphaier. Integral transform solution for heat transfer in parallel-plates microchannels: Combined electroosmotic and pressure driven flows with isothermal walls. *International Communications in Heat and Mass Transfer*, 39(6):769 – 775, 2012.

[16] M. Fakoor-Pakdaman, M. Ahmadi, and M. Bahrami. Unsteady internal forced-convective flow under dynamic time-dependent boundary temperature. *Journal of Thermophysics and Heat Transfer*, 28(3):463–473, 2014.

[17] Diego C. Knupp, Renato M. Cotta, Carolina P. Naveira-Cotta, and Sadik Kakaç. Transient conjugated heat transfer in microchannels: Integral transforms with single domain formulation. *International Journal of Thermal Sciences*, 88:248–257, 2015.

[18] S. Simlandi, N. Berman, and H. Chattopadhyay. Modelling of extrusion process for aluminium A356 alloy. *Solid State Phenomena*, 217-218:188–194, 2015.

[19] Y. Agbessi, L. X. Bu, Y. Béreaux, and J.-Y. Charmeau. Viscoelastic stability in a single-screw channel flow. *AIP Conference Proceedings*, 1960(1):120001, 2018.

[20] H. Ragueb and K. Mansouri. An analytical study of the periodic laminar forced convection of non-newtonian nanofluid flow inside an elliptical duct. *International Journal of Heat and Mass Transfer*, 127(B):469–483, Dec 2018.